Revision 1

Regular article
Word Count: 8309 up to and including "Acknowledgments"

THERMAL EXPANSION OF MINERALS IN THE PYROXENE SYSTEM AND EXAMINATION OF VARIOUS THERMAL EXPANSION MODELS

Guy L. Hovis

Department of Geology and Environmental Geosciences, Lafayette College,

Easton, PA 18042

hovisguy@lafayette.edu

610-908-7438 (cell)

Mario Tribaudino

Dipartimento di Scienze Chimiche, della Vita e della Sostenibilità Ambientale

Università di Parma

Viale G.P. Usberti 157/A

I-43100 Parma, Italy

mario.tribaudino@unipr.it

Amanda Leaman

Department of Geosciences, Utah State University,

Logan, UT 84322

amanda.leaman3@gmail.com

Christine Almer

Department of Geology and Environmental Geoscience, Lafayette College,

Easton, PA 18042

christinealmer@gmail.com

Caitlin Altomare

Shell Exploration & Production Company, 701 Poydras Street,

New Orleans, LA 70139

caitlin.altomare@shell.com

Matthew Morris

Langan Engineering and Environmental Services, 2700 Kelly Road,

Warrington, PA 18976

mdmorris92@outlook.com

Nicole Maksymiw

Environmental Logic, LLC, 11 Princess Road,

Lawrenceville, NJ 08648

nicole.maksymiw12@gmail.com

Derek Morris

2240 51st Street,

Sacramento, CA 95817

morriskderek@gmail.com

Kevin Jackson

Department of Natural Resources and the Environment, University of Connecticut,

Storrs, CT 06269

kevin.jackson@uconn.edu

Brian Scott

Department of Geology and Environmental Geosciences, Lafayette College,

Easton, PA 18042

bscottyus@gmail.com

Gary Tomaino

Specialty Minerals, Inc., 640 North Third Street,

Easton, PA 18042

gary.tomaino@mineralstech.com

Luciana Mantovani

Dipartimento di Scienze Chimiche, della Vita e della Sostenibilità Ambientale

Università di Parma

Viale G.P. Usberti 157/A

I-43100 Parma, Italy

luciana.mantovani@unipr.it

ABSTRACT

In order to examine the effects of chemical composition on thermal expansion in the pyroxene mineral group, X-ray diffraction data have been collected from room temperature to ~925 °C on a chemically diverse group of thirteen pyroxenes, including four orthorhombic and nine monoclinic samples. Additionally, resulting unit-cell volumes computed from the XRD data have proven to be good tests for a large number of thermal expansion models; the physical model by Kroll and coworkers and the empirical one by Fei have been found to be especially useful. Modeling also has allowed the connection of present data, collected at temperatures above 25 °C, to the volume data of other workers for much lower temperatures, well below 0° C, and also extrapolation of values for volume and thermal expansion well beyond the measurement range.

We have found for orthopyroxenes that Fe^{2+}-Mg^{2+} substitution has little effect on thermal expansion coefficients for volume. For clinopyroxenes, however, greater thermal expansion occurs in Ca^{2+}- (diopside, augite, hedenbergite, johannsenite) than in Li^{+}- (spodumene) or Na^{+}-bearing members (jadeite, aegirine, kosmochlor). Present data support the observation that differences in volume thermal

expansion relate primarily to differences in expansion along the b crystallographic axis. This apparently is due to the greater concentration of M1 polyhedra along the b crystallographic axis, where expansion differences can be related to the shared O1-O1 polyhedral edge and inter-oxygen repulsion that is made easier by divalent, as opposed to trivalent, cation occupancy of the M1 crystallographic site.

Keywords: pyroxenes, thermal expansion, modeling

INTRODUCTION

A principal line of research at Lafayette College over more than twenty years has been investigation of the relationship of thermal expansion to the chemical compositions of minerals within specific structural groups. Previously published results include investigation of the entire feldspar system (Hovis et al. 2010, 2008, 1999; Hovis and Graeme-Barber 1997), nepheline – kalsilite feldspathoids (Hovis et al. 2006, 2003), and both F-Cl and F-OH apatites (Hovis et al. 2014, 2015). We now have expanded this work by collecting data on more than fifty mineral specimens covering wide compositional ranges in five additional silicate mineral systems. In the present paper we explore thermal expansion relationships among pyroxenes.

A primary goal of present and previous work has been to provide valuable research experiences for undergraduate students at Lafayette College. Participants in the present work, now all graduated, are coauthors of this paper. The analysis of thermal expansion data has progressed significantly in the last decade, going far beyond questions asked in the previous studies listed above. In fact, high-quality volume (V) - temperature (T) data can be utilized to test various mathematical formulations of V-T data and also incorporated into thermodynamic data bases for the purpose of calculating phase equilibria at elevated temperatures. Even though pyroxene thermal expansion has been studied previously (references appropriate to specific minerals given later), an exploration of physical thermal expansion

This is the peer-reviewed, final accepted version for American Mineralogist, published by the Mineralogical Society of America.
The published version is subject to change. Cite as Authors (Year) Title. American Mineralogist, in press.
DOI: https://doi.org/10.2138/am-2021-7650. http://www.minsocam.org/

models for a systematic collection of pyroxenes is lacking. The current study provides data that can be used for such a purpose, similar to studies on plagioclase and olivine by Tribaudino et al. (2011) and Kroll et al. (2012), respectively.

SAMPLES AND METHODS

Pyroxene samples investigated

A total of four Mg^{2+}-Fe^{2+} orthopyroxenes and nine clinopyroxenes have been investigated. The orthopyroxenes range in composition from nearly-pure-Mg enstatite to pure Fe^{2+} ferrosilite. Monoclinic pyroxenes include three calcic Ca-Mg-Fe specimens ranging in Mg:Fe^{2+} ratio from diopside to "augite" to hedenbergite, and also CaMn johannsenite. Investigated sodic clinopyroxenes include NaAl jadeite, $NaFe^{3+}$ aegirine, and $NaCr^{3+}$ kosmochlor, the latter synthesized in our own laboratory. Additional investigated clinopyroxenes include omphacite, a chemical intermediate between calcic and sodic pyroxenes that crystallizes in a different space group with respect to the others, and LiAl spodumene. Crystallographic, chemical, and other information pertaining to samples studied during this investigation are recorded in Table 1. This will give the reader a feeling for how close or far each sample is from the pertinent end-member composition and also allow compositional comparison among different pyroxenes. Sample compositions from the records of the National Museum of Natural History (Washington, D.C.) and the American Museum of Natural History (New York City), in some cases unpublished, have been important to our work.

Methods

X-ray diffraction measurements were conducted at temperatures ranging from room T to ~928 °C on a PANalytical Emperian X-ray powder diffraction (XRD) system equipped with an Anton-Parr HTK 1200N heating stage. Actual sample temperature was checked periodically by conducting

This is the peer-reviewed, final accepted version for American Mineralogist, published by the Mineralogical Society of America.
The published version is subject to change. Cite as Authors (Year) Title. American Mineralogist, in press.
DOI: https://doi.org/10.2138/am-2021-7650. http://www.minsocam.org/

separate experiments on four different compounds (KNO_3, $KClO_4$, K_2SO_4, $BaCO_3$), which collectively undergo reversible phase transformations at temperatures covering the range ~130 °C to ~815 °C. Each of these samples was X-rayed at small increasing-T increments across its phase transformation, then subsequently cooled in small-T increments across the same transition, then heated again, and so on, while inspecting the X-ray pattern at each temperature. Generally, it was found that the observed temperatures of our experiments were 16 °C to 28 °C above the set temperature displayed on the controller console. The latter stated range in temperature correction probably does not represent real variation in instrumental vs. actual T over time, but likely reflects the standard deviation in average ΔT values that became evident only after performing experiments on our new XRD system over an extended period of time.

Each mineral was subjected to X-rays from room T to a set T of 900 °C at (mostly) 50 °C intervals. X-ray scans were conducted from 15° to 80° 2θ over a 30-minute period at each T, except for some Fe-bearing specimens for which run times of 60 minutes were employed (details in Table 1). All measurements utilized Ni-filtered Cu Kα radiation. Isometric silicon with a 25 °C unit-cell dimension of 5.430825(36) Å, as stated in the NIST certificate for Si Standard Reference Material 640a, was used as an internal standard in all experiments to correct for zero offset. With temperatures calibrated as discussed above, Si peak positions were adjusted for temperature utilizing the thermal expansion data of Parrish (1953), with a linear thermal expansion coefficient for the a unit-cell dimension of 4.1489 x 10^{-4} $Å^{-1}$.

During review of this manuscript, we became aware of a different (and non-linear) formulation for Si thermal expansion employed by Alvaro et al. (2015). To make comparisons with the latter, the Si data of these authors were utilized to determine the unit-cell dimensions of our kosmochlor sample (GH-1558) at temperatures of 22, 272, 522, 722, and 922 °C. Resulting unit-cell volumes for kosmochlor based on the alternative Si data and formulation are generally lower by ~0.2 to 0.4 $Å^3$ than

those reported in Table 2. Any such differences, however, would be systematic across all pyroxenes, in no way affecting comparisons among samples. Note as well that the room-T unit-cell dimension for Si [5.4303(4) Å] reported by Alvaro et al. (ibid) for 297K is slightly different from that stated for the NIST sample used here.

Generally, at the conclusion of an experiment, a room-T X-ray scan was conducted to check for possible sample breakdown. In the case of Fe^{2+}-bearing samples it was common for materials to have changed color to a rusty-red or brown by the conclusion of an experiment, correlating with the identification of hematite in the resulting sample. In such samples, it was common to note deterioration in the quality of X-ray peaks at some point during sample heating. More subtle sample breakdown was indicated by the development of off-trend unit-cell dimensions with increasing T. In our data tables and figures the breakdown of various samples is reflected by shortened temperature ranges ($T < 900$ °C) of reported unit-cell dimensions.

The sample holder utilized for the Anton-Parr stage varied among specimens. In cases where very small amounts of sample were available, the powdered sample (plus Si) was mixed with several drops of iso-amyl acetate on a thin alumina disc, allowed to dry, then mounted on the heating stage. The resulting X-ray patterns of such experiments invariably included corundum peaks, which were ignored in the data reduction. In cases where sufficient amounts of sample were available, powders were placed in a flat-bottomed macor cup, then smoothed off parallel to the top of the cup. Due to the greater thickness of such samples, no extra X-ray peaks from the macor were generated.

Generally, unit-cell dimensions were calculated using the X-ray software of Holland and Redfern (1997), which was downloaded from the unit-cell internet page of Prof. Timothy Holland, University of Cambridge. To avoid automated indexing of low-intensity X-ray peaks related to phase impurities, the *hkl* identities of all peaks were assigned manually, for which both the American Mineralogist Crystal Structure Database (Downs and Hall-Wallace, 2003) and PANalytical Database

This is the peer-reviewed, final accepted version for American Mineralogist, published by the Mineralogical Society of America.
The published version is subject to change. Cite as Authors (Year) Title. American Mineralogist, in press.
DOI: https://doi.org/10.2138/am-2021-7650. http://www.minsocam.org/

were invaluable. Because of this manual indexing, rather than automated indexing now available on various XRD systems, we regard the stated standard deviations of our computed unit-cell dimensions to be realistic. The wavelength of Cu Kα1 radiation for all calculations was taken to be 1.540598 Å, which was the value inherent in PANalytical software.

Our calculated unit-cell dimensions for all pyroxenes are presented in Table 2. Reported standard deviations from the Holland software represent 1σ values, whereas these should be multiplied by 2 or 3 to reflect truer values of the actual uncertainties.

MODELS FOR FITTING VOLUME-TEMPERATURE DATA

Models in the subsequent discussion are named as in Kroll et al. (2012) and Angel et al. (2014). Interested readers also may refer to Angel et al. (2015, 2019 and 2020) and Zaffiro et al. (2019). For a thorough discussion of models for fitting volume-temperature data, we refer readers to supplementary material S1 provided with this paper.

A test of various models utilizing data for jadeite

To test the different formulations for V-T data, we have modelled our results for jadeite sample AMNH 33399. Fits were done on data from 298 through 1195 K, then extrapolated to temperatures below 298 K for comparison with high-quality V-T data between 1.5 and 270 K from the powder neutron diffraction experiments of Knight and Price (2008). Such an exercise provides a good measure of the capability of different models to predict low-temperature behavior and also produces a good estimate of the room-temperature thermal expansion coefficient.

For this test we have utilized a total of five models, two based on physical descriptions (the Einstein linear and Kroll fits), and three empirical models, the first-order (linear) and second-order (quadratic) polynomials of V as f(T), plus the Fei model. Note that experimental data for AMNH 33399

jadeite were rescaled, decreasing all measured V values by 0.40 $Å^3$, in order to merge the low- and high-temperature data sets. Overall results are given in Table 3, as well as Figures 1 and 2. Most models show a good visual fit to the experimental data (Fig. 1), as well as very good values for R^2 (Table 3). An analysis of residuals shows that, on average, these are below 2σ of the average experimental error. The lone exception to this is the fit for the linear model (Table 2), which occurs because V-T data above room T for jadeite and other minerals are normally concave-up. Linear fits to concave-up V-T data give V residuals that are positive at the two ends of the T range, but negative at intermediate temperatures. In fact, analysis of a lower-T (or higher-T) subset of such data produces a different thermal expansion coefficient than does analysis over the entire T range. In the present case, a linear fit to all data for jadeite above room temperature gives a thermal expansion coefficient of 2.69(2) x 10^{-5} K^{-1}, whereas a linear fit limited to data between 298 and 700 K gives the lower value of 2.46(4) x 10^{-5} K^{-1}. This has an important implication, namely that in order to accurately compare the linear thermal expansion coefficients of different mineral samples, it is necessary to utilize data over the same temperature range. This is a critical point, as many studies have utilized linear approximation to compare thermal expansion coefficients.

It is only the Kroll model, with $\theta_E = 537$ K calculated from Holland and Powell (2011) and K' as a refinable parameter, that the V-T curve obtained from present high-T data for jadeite predicts correct volume behavior at $T < 298$ K. This is most likely because it is recast from models that account for non-linear lattice energy vs. T relationships. At the same time, it is fair to point out that alternative choices for θ_E and K' might not have provided equally good volume extrapolation to low temperatures (Fig. 1).

It is important to recognize that extrapolation of V-T data to very low temperatures cannot be accomplished with the Fei model. In this case, as T approaches 0 K, the T^{-2} term causes thermal

expansion to diverge towards infinity. Nevertheless, the Fei model can indeed be utilized to successfully reproduce data within the measurement range of V-T experiments.

Differences among the various models for jadeite are apparent, even within the measurement range, by analysis of the thermal expansion coefficient with temperature. Physical models predict that the thermal expansion coefficient is zero at 0 K and show two inflections with temperature, one concave-up and the other concave-down at lower and higher temperatures, respectively (Kroll et al. 2012). Neither the empirical linear nor polynomial fits fill such requirements, as they are respectively constant and linear with temperature. The empirical Fei model predicts the higher-temperature saturation but fails at lower temperature. It is only the Einstein and Kroll models, then, that can accurately predict expected behavior of α_v with T.

In empirical models, constant (linear model) or linear (polynomial model) thermal expansion is overestimated at room temperature relative to physical models (Fig. 1). The Fei model at higher temperature is close to physical-model predictions, even though for olivine this is not the case (Kroll et al. 2012). Note that thermal expansion coefficients modelled from physical and polynomial fits are generally very similar to one another between 200 and 800 °C.

One possible bias in the Kroll model is the presence of four refinable parameters, which in an unconstrained refinement are highly correlated, having a correlation coefficient >0.85 with V_0 and >0.95 with other parameters. To judge how refinement constraints could affect thermal expansion parameters, values for θ_E and K' were alternately constrained (one each or both) to the experimental values of K'= 4.4 GPa (Nestola et al. 2007) and θ_E = 537 K, the latter based on entropy data tabulated in Holland and Powell (2011). Although an unconstrained fit that includes low-temperature data gives results close to the experimental ones, i.e. θ_E = 490(10) K and K' = 5.6(8) GPa, the unconstrained refinement based on higher-T data alone gives an unreasonable negative value for K'.

This is the peer-reviewed, final accepted version for American Mineralogist, published by the Mineralogical Society of America.
The published version is subject to change. Cite as Authors (Year) Title. American Mineralogist, in press.
DOI: https://doi.org/10.2138/am-2021-7650. http://www.minsocam.org/

ANALYSIS OF PRESENT AND PREVIOUS DATA

As shown for jadeite in Table 4, when alternately fixing either K' or θ_E, the result for the alternate parameter is close to the experimental value. For the analysis of present data and comparison among various pyroxenes, therefore, it seemed reasonable to utilize the Kroll model in which both parameters are fixed, where K' is obtained from pyroxene high-P equations of state and θ_E from the data of Holland and Powell (2011), with linear interpolation between end members. Consider again that such a constrained fit for jadeite, based on present data above room T, did well in predicting independently-measured low-T data (Fig. 2).

In addition, we have employed the Fei equation in V-T fits, using full expansion in cases where refinements gave significant values for a_0, a_1, and a_2 parameters, which occurred in five of 12 samples, namely enstatite, diopside, jadeite, kosmochlor and augite. In other pyroxenes only the a_0 and a_1 parameters were refined, resulting in second-order polynomials. For hedenbergite the a_1 parameter was smaller than the error, producing a close-to-linear fit. Results of these calculations are shown in Table 5.

One may also compare values of $\chi 2$ for fits to the same dataset using both the Fei and Kroll models. Because $\chi 2$ reflects agreement of any model with the data, one might expect it to be similar for the two models. On the other hand, because the Fei fit is simply an empirical best-fit to the data, one would expect better agreement for the latter, which is indeed observed (Table 6). Although higher values in $\chi 2$ for the physical model could indicate incorrect choices for physical constants K' and θ_E, Table 6 shows both $\chi 2$ values and room-temperature volumes for the two models to be very similar.

Another comparison of the two models comes from calculating thermal expansion at a given temperature. We did this for 298 and 1073 K, where thermal expansion for the Kroll model was obtained directly from the code and that for Fei by deriving the fit at the given temperature. The greatest difference between the two models was observed for hedenbergite, for which the almost-linear

fit (possibly related to the lower quality of the data) overshoots at higher temperatures and underestimates at lower temperatures. At 298 K the two models differ most, whereas at 1073 K there is good agreement (Fig. 3). This is consistent with our observations for jadeite, for which there is good agreement among thermal expansion coefficients based on different models for the temperature range from 500 to 1100 K. Indeed, differences between the models at 298 K are expected, as the empirical Fei model is less effective in describing low-T thermal expansion, with α_T becoming infinite at 0 K. Note as well that a larger difference at 298 K between the Fei and Kroll models is observed for omphacite, aegirine and spodumene, for which data did not allow refinement of all Fei parameters.

Orthopyroxenes from enstatite to ferrosilite

Because they are major rock forming minerals, several papers have been published on the thermal expansion of orthopyroxenes studied via X-ray diffraction (Jackson et al. 2003, Hugh-Jones 1997, Zhao et al. 1995, Yang and Ghose 1994, Frisillo and Buljan 1972, Smyth 1973, Sueno et al. 1976) or dilatometric methods (Dietrich and Arndt 1982, Sarver and Hummell 1962). V/V_0 ratios for enstatite are shown in Figure 4 from the most recent investigations that utilized X-ray diffraction techniques. Note that the use of V/V_0 to compare end-member thermal expansion, rather than volume alone, mitigates small differences in unit-cell parameters at room temperature that are the result of chemical impurities and/or differences in laboratory techniques. The data of Jackson et al. (2003) show relatively high scatter, which is likely due to lower precision inherent in the EDX detection methods used by these workers. This prevented data analysis using a physical equation, so a linear fit to their data was done instead. Note that the latter results deviate above 1000 K from those of other investigations. Unfortunately, high scatter in the data of Hugh-Jones (1997), as well, prevented useful analysis using present methods. As for current enstatite data (Fig. 5), refinement using the Fei equation indicates that all parameters are statistically significant. Moreover, the latter closely connect with those

of previous work by Yang and Ghose (1994). The room-temperature thermal expansion obtained for this study agrees well with that from Yang and Ghose (α_{298} = 2.602(9) and 2.62(2) x 10^{-5} K^{-1}).

Natural orthopyroxenes show some degree of Fe^{2+}-for-Mg substitution, so it is pertinent to ask what effect such substitution has on thermal expansion. Despite a large number of experiments, data from the literature that address this question show a high degree of scatter, with thermal expansion values ranging from 2.4 to 4.77 x 10^{-5} K^{-1} for orthoenstatite and 2.03 to 3.93 x 10^{-5} K^{-1} for orthoferrosilite (Hugh-Jones 1997). The latter paper also compares the thermal expansion of clino- and orthoenstatite to that of ferrosilite, concluding for the two orthorhombic phases that ferrosilite shows lower thermal expansion, 2.75(15) x 10^{-5} K^{-1} vs. 3.22 (11) x 10^{-5} K^{-1} based on linear fits to data between 293 and 900 K. The data of Yang and Ghose (1994) for intermediate enstatite-ferrosilite solid solutions, on the other hand, indicate that Fe^{2+}-for-Mg substitution increases thermal expansion at room temperature, but slightly decreases the latter at the highest temperatures.

Analysis of present data for end-member orthoferrosilite using the Kroll equation is hindered by sample degradation (due to iron oxidation) above 700 K, a temperature above which Hugh-Jones (1997) also observed anomalous decrease in thermal expansion. To address this, we utilized the Kroll equation to fit present data as merged with those from Sueno et al. (1976). Results confirm the findings of Yang and Ghose (1994) that at about 700 K the thermal expansion coefficient becomes greater in enstatite, but that between 500 and 1100 K the difference is hardly significant. This is consistent with results between 298 and 700 K for present samples having intermediate Mg:Fe ratios (Fig 6). Like ferrosilite, the iron-richer orthopyroxenes show sharp XRD peaks at low T that strongly degrade with rising temperature (thus the reporting of lower-T unit-cell data only). Linear fits to intermediate orthopyroxenes between 298 and 700 K may be compared with those for ferrosilite and enstatite. Within error, changes in volume due to the presence of Fe^{2+} are hardly distinguishable, with slightly higher expansion for ferrosilite. Note that the higher standard deviation of data for enstatite (Fig. 6)

This is the peer-reviewed, final accepted version for American Mineralogist, published by the Mineralogical Society of America.
The published version is subject to change. Cite as Authors (Year) Title. American Mineralogist, in press.
DOI: https://doi.org/10.2138/am-2021-7650. http://www.minsocam.org/

relates to the greater curvature of its V-T trend, corresponding to a predictable greater increase in thermal expansion, not to scatter in the data.

Calcic clinopyroxenes

Diopside. Diopside ($CaMgSi_2O_6$) is an important end-member pyroxene having the typical structure of group members possessing C 2/c space group symmetry. Indeed, it was on diopside that the first investigation of pyroxene thermal expansion was accomplished up to 1273K by Kozu and Ueda (1933) using dilatometric methods. Initial studies on diopside thermal expansion using X-ray diffraction were reported by Deganello (1973) and Cameron et al. (1973) in their comprehensive analysis of clinopyroxene crystal structures at high temperature. Because these studies determined unit-cell dimensions at just four and five temperatures, respectively, volume data were fit according to a linear model. Later work up to 800°C by Finger and Ohashi (1976) measured diopside unit-cell dimensions at a closer T interval and examined the strain tensor with temperature. Richet et al. (1998) measured unit-cell dimensions to just below diopside's melting point in parallel with high-T in-situ Raman spectroscopy. More recently, Ferrari et al. (2014) and Pandolfo et al. (2015) provided unit-cell data at closely spaced temperatures, allowing data analysis using both the Berman polynomial and empirical Holland models, with no attempt at a physical model. Results from the latter investigations (Fig. 7) are more-or-less scattered but follow similar trends, except for the higher-T data of Richet et al. (1998) that deviate significantly from the other studies above 900 K; the latter negates development of a single equation of state for their data at both low- and high-temperatures.

A fit of present diopside V-T data shows significance for all parameters of the Fei equation (Table 6). In the same table, the Kroll fit shows higher residuals and a poorer weighted χ^2 parameter than the latter, which could indicate that the physical parameters fixed for θ_E or K' are either over- or underestimated. As shown by Xu et al. (2019), several determinations of K' for diopside range from 6.8

(Tribaudino et al. 2000) to 3.8 (Thompson and Downs 2008). A fit to present data using the 3.8 value is somewhat better, with weighted χ^2 very close to that from a fit using the Fei equation.

Hedenbergite. Several studies have been accomplished on hedenbergite using single-crystal techniques (Cameron et al 1973, Tribaudino et al 2008b, Ferrari et al 2014). Cameron et al. (1973) and Tribaudino et al. (2008b) fit V-T data linearly; an application of a polynomial fit to the 2008 data shows a concave-down V-T curve that predicts an unrealistic decrease in the thermal expansion coefficient with T. Results from the more recent study by Ferrari et al. (2014) utilized a polynomial fit, showing an upward concave behavior for data up to 773 K. Figure 7 demonstrates that data from the three studies are closely grouped up to 800K, a temperature at which data from present work reflect sample degradation. Note that some scatter is shown for data at higher temperature by both Cameron et al. (1973) and Tribaudino et al. (2008b).

Comparison of data for diopside to those of hedenbergite is pertinent, as many natural clinopyroxenes are solid solutions between these end members. Ferrari et al. (2014) showed that at room temperature thermal expansion coefficients for the two pyroxenes are equal. That Fe-Mg exchange in the M1 site does not measurably affect thermal expansion is reflected by equivalence of the two polynomial coefficients in Berman fits for the two minerals (Table 6, Ferrari et al. 2014).

Although Kroll fits to our diopside and hedenbergite data show similar results, those for hedenbergite are based on a more limited T range and also have higher errors that are likely the result of peak broadening due to chemical zoning in the present sample. Clarification may reside in present data for augitic pyroxene (NMNH 16168) of intermediate composition ($Di_{44}Hd_{56}$), for which data quality is comparable to that of diopside. Thermal expansion for this specimen is similar to those of the end members, although below 500 K $\alpha_{hed}>\alpha_{aug}>\alpha_{di}$, whereas at higher temperatures the opposite is true. Such differences, however, are hardly measurable and in general confirm that thermal expansion is little affected by Mg-Fe^{2+} substitution.

This is the peer-reviewed, final accepted version for American Mineralogist, published by the Mineralogical Society of America.
The published version is subject to change. Cite as Authors (Year) Title. American Mineralogist, in press.
DOI: https://doi.org/10.2138/am-2021-7650. http://www.minsocam.org/

Johannsenite. To our knowledge, no previous high temperature in situ determination of the thermal expansion of johansennite have been done. We expected that the V-T measurements on johannsenite ($CaMnSi_2O_6$; specimen NMNH 97484) should have resulted simply in determination of the effect of Mn^{2+}-for-Mg/Fe^{2+} M1-site substitution on thermal expansion. However, present data for johannsenite show significant peak broadening at temperatures above ~400 °C, which is most likely due to onset of the phase transformation from johannsenite to bustamite (reported by Angel 1984), even though the major XRD peaks for johannsenite continue to higher temperatures. The discontinuity in unit-cell data are shown particularly well on a plot of the a unit-cell dimension against temperature (Fig. 8). Because of this issue, analysis of present data is limited to temperatures below 400 °C. A linear fit to such data indicates a higher thermal expansion coefficient for johannsenite than for either diopside or hedenbergite, where the linear thermal expansion coefficient for johannsenite (α_v=3.12(4) x 10^{-5} K^{-1}) between 25 and 400 °C is within two standard deviations of the linear thermal expansion calculated for diopside, augite and hedenbergite (α_v=2.98(7), 2.99(3), 3.02(5) x 10^{-5} K^{-1}).

Sodic clinopyroxenes

Jadeite. Sodium pyroxenes have been widely studied as major phases in both alkaline volcanics and high-pressure metamorphic rocks. Among these, jadeite ($NaAlSi_2O_6$) has been the most investigated pyroxene at high P-T. To our knowledge, Cameron et al. (1973) performed the first thermal expansion study on jadeite, followed by work at both high P and T by Zhao et al. (1997), who fit their high-T data to a Fei equation excluding the T^{-2} term. Synthetic end-member jadeite was studied by Tribaudino et al. (2008b), whose work also included intermediate compositions of jadeite-hedenbergite and jadeite-aegirine series. This work demonstrated that Al-Fe^{3+} exchange between jadeite and aegirine has little effect on thermal expansion. On the other hand, coupled $CaFe^{2+}$-NaAl exchange from hedenbergite to jadeite does indeed increase thermal expansion. Pandolfo et al. (2015)

measured unit-cell dimensions along a jadeite-diopside series; the fit to data using a Berman equation indicated that thermal expansion at room temperature decreased with increasing jadeite component. Additionally, Knight and Price (2008) used time-of-flight neutron diffraction to study unit-cell dimensions from room temperature to 1.5 K. The data were fit according to the Wallace formulation of the Einstein equation. As shown in Figure 9, this work and previous investigations match a similar trend. In detail, it appears that Cameron et al. (1973) slightly underestimate thermal expansion relative to more recent investigations.

Aegirine. The effect of Fe^{3+}-Al exchange on thermal expansion in sodic pyroxenes can be studied via data for the jadeite-aegirine series. Aegirine previously has been investigated at high temperature by both Cameron et al. (1973) and Tribaudino et al. (2008b). No significant difference in thermal expansion for jadeite, aegirine, or their intermediate compositions was found. Note that Redhammer et al. (2006) also investigated aegirine at low T, but with particular focus on crystal structures and Mössbauer behavior. Figure 10 shows that the data of Cameron et al. (1973) and Tribaudino et al. (2008b) are somewhat scattered, whereas those from the current study are between the others and more regular in variation. Present results, fit with a Kroll equation together with the low-temperature data for aegirine (Redhammer et al. 2006), confirm similarity in the thermal expansion of jadeite and aegirine. Just as for ferrosilite and hedenbergite, the Fe-bearing component shows slightly higher thermal expansion at lower temperature, but lower expansion at higher temperature.

Kosmochlor. The effect of Cr^{3+} on thermal expansion in Na-pyroxenes can be studied utilizing kosmochlor, ($NaCrSi_2O_6$). This component, most important in meteoritic pyroxenes, was first investigated by Cameron et al. (1973), whose data at three temperatures indicate a significantly lower average thermal expansion than for either jadeite or aegirine. A Kroll fit on V-T data at nineteen temperatures between 298 to 1195 K from the present work, combined with low-temperature unit-cell

This is the peer-reviewed, final accepted version for American Mineralogist, published by the Mineralogical Society of America.
The published version is subject to change. Cite as Authors (Year) Title. American Mineralogist, in press.
DOI: https://doi.org/10.2138/am-2021-7650. http://www.minsocam.org/

data at 10 K of Nenert et al. (2010), demonstrates that thermal expansion is indeed less in kosmochlor than in either jadeite or aegirine over all temperatures.

Na-Ca/Al-Mg-Fe pyroxenes

Omphacite. In order to determine the effect of coupled Na-Ca and Al-(Mg,Fe) pyroxene substitution on thermal expansion, we include V-T data from the present study on natural omphacite, $(Ca_{0.50}Na_{0.50})(Al_{0.43}Mg_{0.48}Fe^{2+}_{0.01}Fe^{3+}_{0.05}Cr_{0.04})Si_2O_6$, essentially intermediate in composition between diopside and jadeite. Figure 9 demonstrates that thermal expansion coefficients for this specimen are indeed intermediate relative to those of the latter minerals. This also confirms the observation of lower thermal expansion for sodic pyroxenes at any temperature.

Lithium pyroxene

Spodumene. In natural clinopyroxenes the M2 site is generally filled by Ca or Na, with or without some Mg and/or Fe^{2+}. Only Li can fully exchange for Na as a monovalent cation in the M2 site. Several studies collected diffraction data at temperatures higher or lower than 298 K on synthetic Li-Fe, Li-Cr or LiNi pyroxenes with silicon or germanium in the T site (Behruzi et al. 1984, Redhammer et al. 2001, 2004, 2015, 2016, 2017, Camara et al. 2009, Tribaudino et al. 2009), aiming to understand phase transitions and the magnetic behavior of these phases. Such studies, however, excluded the only naturally occurring Li-pyroxene end member, spodumene ($LiAlSi_2O_6$). Until now, the only published high-temperature data on spodumene were collected by Cameron et al. (1973), supplemented by the low-T data of Tribaudino et al. (2003) at 54 K from a single-crystal neutron diffraction experiment. The data of Cameron et al. (1973) at four temperatures demonstrate that spodumene has lower thermal expansion than either jadeite or kosmochlor. A Kroll fit to present data at

nineteen temperatures (Figure 11) confirms that spodumene has lower thermal expansion than jadeite, but does not demonstrate a difference with kosmochlor (compare Figs. 11 and 10b).

Al-bearing-orthopyroxene and Ca-Tschermak pyroxene

Other than in pyroxenes with a monovalent cation in the M2 site, such as Li and Na, Al enters clino- and orthopyroxenes via a coupled Ca-Tschermak substitution of Al for Mg, Fe and Si in M1 and T sites. This substitution was investigated in present work through V-T measurements on a natural Al-bearing orthopyroxene. A fit with the Kroll equation demonstrates that for T > 298 K, the Al-bearing pyroxene shows lower thermal expansion than either enstatite or ferrosilite.

In the present work, we have not investigated the effect of Tschermak substitution, in clinopyroxenes. Previous studies, however, do include high-temperature V-T data for synthetic Ca-Tschermak ($CaAl_2SiO_6$, or CaTs, Haselton et al. 1984), as well as for intermediate solid solutions $CaTs_{50}Di_{50}$ and $CaTs_{30}Di_{70}$ (Tribaudino 1996). Both investigations show large experimental errors, which limits data analysis to an assumption of constant thermal expansion (Fig. 12). Results indicate that Tschermak substitution decreases thermal expansion, which confirms previous observations that thermal expansion is less in pyroxenes having a trivalent cation in the M1 site (e.g. Cameron et al. 1973).

DISCUSSION

General trends in the thermal expansion of pyroxenes

The above results show significant differences among the investigated end members. These differences may in part be interpreted in terms of crystal-chemical distinctions between the clino- and orthopyroxene groups. A plot of unit-cell volume vs. thermal expansion coefficient at 298 K (Fig. 13) demonstrates for most clinopyroxenes that thermal expansion is directly proportional to unit-cell

volume. The lone exceptions to the latter are aegirine and kosmochlor, which show lower room-T unit cells than those expected from room-T thermal expansion coefficient. Note as well that orthopyroxenes generally show greater thermal expansion than clinopyroxenes based on room-T unit-cell volume. This figure also demonstrates that Ca-pyroxenes show higher thermal expansion than either Na- or Li- end members.

The mechanism for thermal expansion in pyroxenes has been discussed in many of the papers listed above. Beginning with the work of Finger and Ohashi (1976), interpretation has involved analysis of axial thermal expansion in terms of size and orientation of the strain ellipsoid based on the strain tensor, with focus on structural changes that occur along greater and lesser deformation directions. Interested readers may refer to such literature for discussions of specific pyroxenes. Generally, however, higher thermal expansion has been found to occur along the b crystallographic axis, with the other deformation axes on (010). Tribaudino and Mantovani (2014) have pointed out that deformation with temperature on the (010) plane does differ slightly among pyroxenes, but agree that the main differences in thermal expansion are related to differences in deformation along b.

In previous investigations deformation with temperature was studied simply by comparing high-T with low-T unit cells, without focus on changes in the size and orientation of the strain tensor. Because thermal expansion coefficients change with temperature, axial deformation should change as well. Therefore, it will be informative to model such changes in order to understand the mechanics of volume behavior.

Thermal strain with temperature

The thermal strain tensor shows the directions of deformation with temperature in a given crystal. The geometric expression of thermal expansion is a property ellipsoid whose semi-axes are the eigenvalues of the tensor. Orientation of the thermal ellipsoid is constrained by symmetry. For

This is the peer-reviewed, final accepted version for American Mineralogist, published by the Mineralogical Society of America.
The published version is subject to change. Cite as Authors (Year) Title. American Mineralogist, in press.
DOI: https://doi.org/10.2138/am-2021-7650. http://www.minsocam.org/

orthorhombic substances axes of the ellipsoid coincide with the crystallographic axes, and the eigenvalues can readily be obtained from the ratio of high- to low-temperature unit-cell parameters. In monoclinic pyroxenes this applies only to the b axis, whereas on (010) orientations of the other axes are not fixed. The thermal strain tensor is obtained by comparing high- and low-temperature unit cells; eigenvalues of the diagonalized tensor are the axial strain values. Program strain by Ohashi (1982), now improved and implemented by the Angel et al. (2014) EOSfit7c program, has been used to determine the orientation and size of the strain axes in monoclinic pyroxenes.

To investigate the changes of strain with temperature, we have modelled the unit-cell parameters with a second-order polynomial. Although this approach is not exactly correct, as a physical model should better fit the data, it does provide a reasonable description of how the individual cell parameters change with temperature. As discussed above, the derivative of the polynomial is a straight line whose slope enables modelling of the extent of changes with temperature for a given component. For monoclinic symmetry there are just four non-zero components in the strain tensor, all of which can be obtained at each temperature as follows:

(12) $a_{11} \approx 1/a(\partial a/\partial T) + (\partial \beta^*/\partial T)\cot \beta^*$

(13) $a_{22} \approx 1/b(\partial b/\partial T)$

(14) $a_{33} \approx 1/c(\partial c/dT)$

(15) $a_{13} \approx 0.5 \cot \beta^*[1/c(\partial c/dT) - 1/a(\partial a/dT)] + 0.5(\partial \beta^*/\partial T)$

Here we follow the Brown setting (Angel et al. 2014), that is, for monoclinic symmetry the reference system is $a_{11} \equiv$ a*, $a_{22} \equiv$ b, $a_{33} \equiv$ c. For orthorhombic symmetry the angular components are missing and a_{13} is 0. The strain was calculated from unit cells based on polynomial modeling using the EosFitc code of Angel et al. (2014). Results are reported in Figure 14.

This is the peer-reviewed, final accepted version for American Mineralogist, published by the Mineralogical Society of America.
The published version is subject to change. Cite as Authors (Year) Title. American Mineralogist, in press.
DOI: https://doi.org/10.2138/am-2021-7650. http://www.minsocam.org/

Axial to volume expansion contribution and crystallographic features

Clinopyroxenes. As shown in Figure 14, all investigated clinopyroxenes show greater thermal expansion along the b axis and less along the a* and c axes. For members with Ca in the M2 site expansion along b is greater than for those having Na in M2, yet similar to the latter in other structural directions. This confirms the observation by Tribaudino and Mantovani (2014) that higher expansion along b accounts for the greater overall volume expansion in Ca-bearing vs. Na-bearing pyroxenes. Differences in expansion along the b axis are related to greater contribution to thermal expansion by M1 octahedra along this axis. Expansion is higher when M1 polyhedra are occupied by divalent cations as a result of weaker bonding relative to polyhedra occupied by trivalent cations, as is the case in sodic pyroxenes. This point seems to be confirmed in spodumene, with Al^{3+} in the M1 polyhedron but Li^{+} instead of Na^{+} in the M2 polyhedron, which produces thermal expansion along b that is similar to that in jadeite. In omphacite, with intermediate trivalent:divalent ratio in M1, one observes intermediate thermal expansion.

Thermal expansion along the b axis changes more with temperature in Ca-pyroxenes than in Li- or Na-pyroxenes such that at higher temperatures the difference in thermal expansion between Ca vs. Li or Na pyroxenes increases. Because other components show only small changes with temperature, changes along the b axis account also for the steeper change in thermal expansion at higher temperature in calcic vs. sodic pyroxenes, just as for diopside vs. jadeite; once again, omphacite shows intermediate expansion behavior relative to the latter (Fig. 14).

Thermal expansion along the c direction (a_{33}) ranges from 0.4 to 0.7 x 10^{-5} K^{-1} and changes little with temperature. This comes from the relative stiffness of the tetrahedral chains, which are parallel to c, and can be elongated-simply by kinking of the latter. Such kinking with temperature is quite small in C2/c pyroxenes (at most an increase of 3° for hedenbergite between 25 and 1000 °C; Cameron et al 1973), so the increase along c is small as well. Moreover, the axial expansion along c

This is the peer-reviewed, final accepted version for American Mineralogist, published by the Mineralogical Society of America.
The published version is subject to change. Cite as Authors (Year) Title. American Mineralogist, in press.
DOI: https://doi.org/10.2138/am-2021-7650. http://www.minsocam.org/

does not change with temperature, even decreasing in augite and aegirine. Thermal expansion normal to the tetrahedral chain plane, i.e. (100), is reflected by the a_{11} value. In this direction deformation is similar at room temperature, ~0.7 x 10^{-5} K^{-1} (0.5 in augite and spodumene). This increases with temperature, except in hedenbergite. It is not clear whether the decrease in hedenbergite is due to ~~a~~ sample degradation associated with the onset of transformation to bustamite or some other behavior.

In sodic pyroxenes thermal expansion is more isotropic than in Ca-bearing ones, this related to lower expansion along the b axis. Another difference, previously noted, lies in different deformation on the (010) plane. For jadeite vs. aegirine thermal expansion along the b and c axes at lower temperature is greater in aegirine. As temperature increases, however, jadeite shows greater increase along b, while thermal expansion in aegirine decreases along c. This likely accounts for the inversion in thermal expansion between aegirine and jadeite at high temperature.

The a_{13} component is present only in monoclinic pyroxenes and accounts for changes in the interaxial angle β. To describe the parameter in terms of structural features, it is useful to determine the orientation of the strain ellipsoid onto the (010) plane. This was done on data between 25 and approximately 420°C, the temperature at which johansennite shows early signs of the transition to bustamite and hedenbergite data degrades apparently due to iron oxidation. Results are reported in Table 7. As shown in Figure 15, Ca-bearing pyroxenes show a very similar orientation of the deformation onto the (010) plane, with the major deformation at about 140° from the c axis. In sodic pyroxenes the major deformation occurs along a direction close to a*, whereas in Li-bearing spodumene it occurs in a direction normal to that in Ca-pyroxenes. This pattern has been interpreted by Tribaudino and Mantovani (2014) to be related to the shift in tetrahedral chains, as reflected by changes in the β parameter, which (a) increases with temperature in Ca-pyroxenes, (b) is constant in jadeite, and (c) decreases in aegirine, kosmochlor, and (especially) spodumene. Orientation of the larger

This is the peer-reviewed, final accepted version for American Mineralogist, published by the Mineralogical Society of America.
The published version is subject to change. Cite as Authors (Year) Title. American Mineralogist, in press.
DOI: https://doi.org/10.2138/am-2021-7650. http://www.minsocam.org/

deformation on (010) changes somewhat at higher temperature, with an approach in diopside to the a axis.

Orthopyroxenes. For orthopyroxenes modelling of axial thermal expansion with temperature was possible only for enstatite, $En_{75}Fs_{25}$, and the Al-bearing sample, whereas the ferrosilite end member produced good-quality data over a greatly shortened temperature range that allowed only linear fits to cell-parameter data and thus constant axial expansion. For the $En_{75}Fs_{25}$ sample unit-cell parameters above 500°C show an apparent decrease in thermal expansion at higher temperature along the b axis, whereas other orthopyroxenes show no such trend (Fig. 16). A decrease in thermal expansion along b at higher temperature was observed also in Fs-richer samples by Yang and Ghose (1994). For ortho- vs. clinopyroxenes, thermal expansion along the b axis is similar, but along c is greater in orthopyroxenes, the latter correlating with elongation of the tetrahedral chains. Thermal expansion along the a axis in orthopyroxenes is relatively minor and similar to that along the structurally-corresponding a* direction in clinopyroxenes. The higher expansion along c provides a rationale for the higher-than-predicted unit-cell volume expansion in ortho- vs. clinopyroxenes.

It is an interesting exercise to compare thermal expansion along the various crystallographic axes for all investigated orthopyroxenes. Generally, clinopyroxenes exhibit greater expansion along the b axis at lower temperature, but in enstatite, $En_{75}Fs_{25}$, and the Al-bearing orthopyroxene expansion along the c axis rivals or exceeds that along b at higher temperatures. Greater thermal expansion along the c axis at elevated temperature was also found in Mn-bearing pyroxene by Scandolo et al 2015, and in Fe-Mg orthopyroxenes by Yang and Ghose (1994). This contrasts with the nearly constant expansion behavior of c with temperature in clinopyroxenes. Because c is the direction along which tetrahedral and octahedral chains are elongated, this suggests progressively greater deformation along the tetrahedral chain with increasing T. Indeed, because the tetrahedra in pyroxenes show only minor changes in size with temperature, any expansion along the c axis requires rearrangement of the

tetrahedral chain. This implies progressive opening of the O3-O3-O3 kinking angle, as suggested in several previous papers (e.g., Thompson and Downs 2004). *C*2/*c* clinopyroxenes have a single tetrahedral chain by symmetry that shows only a minor increase (3° at most) in the kinking angle with temperature (Cameron et al. 1973). *Pbca* orthopyroxenes, on the other hand, have two symmetrically independent tetrahedral chains, one that is highly kinked at room temperature, opening to 12° at higher T in a non-linear fashion (e.g. Smyth 1973), perhaps leading to a phase transition. Consequently, the c axis and thus volume increase is more in orthopyroxenes. Such change is related to the P-type structure. Indeed, in Ca-poor pigeonitic $P2_1/c$ pyroxenes, we find similar behavior at high temperature, with strong change in thermal expansion along the c axis, and values along the a and b axes comparable to those of other clinopyroxenes, showing little change with temperature. This, in fact, has been observed for a synthetic $Di_{15}En_{85}$ pyroxene (Tribaudino et al. 2002) in connection with the high-temperature phase transition to C2/c symmetry (Fig. 17).

SUMMARY AND CONCLUSIONS

The initial aim of this study was (1) to collect both accurate and precise volume data as a function of temperature on a compositionally diverse set of pyroxene minerals and (2) to understand the reasons for differences in thermal expansion among various members of this mineral group. Toward these ends, we utilized NIST 640a silicon as an internal standard in all unit-cell calculations. We also checked instrumental temperatures through separate XRD experiments on materials that exhibit second-order phase transformations at known temperatures. And, of course, we have provided chemical data for the various samples.

Altogether we studied thirteen different samples, four orthopyroxenes and nine clinopyroxenes. Complete unit-cell data sets at ~50 °C intervals from room temperature to ~925 °C are the result of computations for seven of the thirteen samples, one orthopyroxene and six clinopyroxenes. For Fe^{2+}-

and Mn^{2+}-bearing pyroxene samples, shortened reported data ranges are the result of iron or manganese oxidation at elevated temperature, and in the case of johannsenite also the apparent onset of phase transformation to bustamite. Overall, the reported data show high precision and smooth variation with temperature (Table 2, Fig. 2). Note that the present study provides data at closer temperature intervals than some of the previous work on these minerals, which has proven to be especially advantageous in modelling V-T relationships.

For minerals having volume data over extensive temperature ranges, the thermal expansion models of Kroll et al. (2012) and Fei (1995) have been found to be particularly useful, with computations aided considerably by the software of Angel et al. (2014). The modelling of V-T relations also connects present data collected above room temperature to those of previous investigators for temperatures well below 0 °C, as well as to tabulated pyroxene thermodynamic data such as those given in Holland and Powell (2011).

Relative to the chemical effects on thermal expansion of pyroxene-group minerals, the substitution of Fe^{2+} for Mg^{2+} in orthopyroxenes seems to have only minimal effect on thermal expansion coefficients for volume. This is not the case for clinopyroxenes, however, which show greater thermal expansion for Ca^{2+}- as opposed to Li^{+}- and Na^{+}-bearing members. As observed by previous workers, the magnitudes of thermal expansion coefficients for volume are associated primarily with differences in expansion along the b crystallographic axis. Tribaudino and Mantovani (2014) note that this is largely the result of the greater concentration of M1 polyhedra along the b axis, where extension of the O1-O1 shared polyhedral edge resulting from inter-oxygen repulsion is made easier by divalent, as opposed to trivalent, cation occupancy of the M1 site. Present data for Ca^{2+}- vs. Na^{+}- or Li^{+}-bearing pyroxenes are indeed consistent with this idea, as is the relatively small effect of Fe^{2+}-Mg^{2+} substitution on thermal expansion among the various orthopyroxenes, as well the relative dampening of expansion in our Al-bearing orthopyroxene sample.

With the completion of work on pyroxenes, we look forward to presenting our thermal expansion data for minerals in the garnet, olivine, amphibole, and tourmaline systems.

IMPLICATIONS

The most obvious implication of the present work is the ability to update existing datasets used to calculate thermodynamic equilibria of mineral assemblages, for example, using Thermocalc (Holland and Powell 2011) or Perple_X (Connoly 2005). Comparison with previous papers infers good data precision and accuracy, confirmed by recent determinations on two pyroxene phases, diopside (Ferrari et al. (2014) and jadeite (Pandolfo et al. 2015). We also have demonstrated that physical thermal expansion models can be used to extrapolate molar volume beyond the temperature limits imposed by laboratory heating devices.

In addition, we have contributed to modelling of the thermal tensor with temperature. In previous investigations, except that of Yang and Ghose (1994) for orthopyroxenes, axial thermal expansion was modelled by linear extrapolation, and the thermal expansion tensor was not determined. Yet the anisotropy of thermal expansion and its changes with temperature play an important role in modelling the hydrostatic vs. non-hydrostatic pressure field of inclusions in minerals (e.g., Murri et al. 2019, Mazzucchelli et al. 2019, Alvaro et al. 2020) and in modelling the high pressure and temperature equation of state. For instance, Angel et al. (2019) have shown that the Mie-Gruneisen equation, most commonly used to model volume at high pressure and temperature, has strong limitations for samples in which the effects of P vs. T on the strain axes are not opposite, in turn inducing anisotropic behavior of thermal pressure.

ACKNOWLEDGMENTS

GH sincerely thanks the Earth Sciences Division of the U.S. National Science Foundation for grants EAR-1019809 and EAR-1028953 that were necessary for the performance of this research. He also thanks John Wilson of the Department of Geology and Environmental Geosciences and William Yox of Information Technology Services of Lafayette College for generous help during the course of this work.

Equally necessary for this work were the pyroxene samples provided by a number of sources, including the U.S. National Museum of Natural History (Jeffrey Post, Paul Pohwat) and the American Museum of Natural History (George Harlow), whose specimens are designated as NMNH and AMNH, respectively, and also Donald Lindsley of Stony Brook University. For the larger project on five mineral systems we also are fortunate to have received specimens from Frank Hawthorne (University of Manitoba), George Rossman (California Institute of Technology), Anthony Law (formerly of Oxford University), M. Darby Dyar (Mt. Holyoke College), and Pascal Richet (IPGP, Paris). We thank these institutions and individuals for their generosity.

REFERENCES CITED

Alvaro, M., Angel, R.J., Marciano, C., Milani, S., Scandolo, L., Mazzucchelli, M.L., Zaffiro, G., Rustioni, G., Briccola, M., Domeneghetti, M.C., Nestola, F. (2015) A new micro-furnace for in situ high-temperature single-crystal X-ray diffraction measurements. Journal of Applied Crystallography, 48, 1192-1200.

Alvaro, M., Mazzucchelli, M.L., Angel, R.J., Murri, M., Campomenosi, N., Scambelluri, M., Nestola, F., Korsakov, A., Tomilenko, A.A., Marone, F., Morana, M. (2020) Fossil subduction recorded by quartz from the coesite stability field. Geology, 48, 24-28.

Anderson, O.L., Isaak, D., and Oda, H.T. (1992) High temperature elastic constant data on minerals relevant to geophysics. Review of Geophysics, 30, 57–92

Angel, R.J. (1984) The experimental determination of the johannsenite-bustamite equilibrium inversion boundary. Contributions to Mineralogy and Petrology, 85, 272-278.

Angel, R.J., and Jackson, J.M. (2002) Elasticity and equation of state of orthoenstatite, $MgSiO_3$. American Mineralogist, 87, 558–561

Angel, R.J., Gonzalez-Platas, J., and Alvaro, M. (2014) EosFit7c and a Fortran module (library) for equation of state calculations. Zeitschrift für Kristallographie - Crystalline Materials, 229, 405-419.

Angel, R.J., Nimis, P., Mazzucchelli, M.L., Alvaro, M., Nestola, F. (2015) How large are departures from lithostatic pressure? Constraints from host-inclusion elasticity. Journal of Metamorphic Geology, 33 (8), pp. 801-813.

Angel, R.J., Miozzi, F., and Alvaro, M. (2019) Limits to the validity of thermal-pressure equations of state. Minerals, 9, 562.

Angel, R.J., Alvaro, M., Schmid-Beurmann, P., Kroll, H. (2020) Commentary on Constraints on the Equations of State of stiff anisotropic minerals: Rutile, and the implications for rutile elastic barometry [Miner. Mag. 83 (2019) pp. 339-347] Mineralogical Magazine, 83, 1-3.

Arlt, T., and Angel, R. (2000) Displacive phase transitions in *C*-centered clinopyroxenes: spodumene, $LiScSi_2O_6$ and $ZnSiO_3$. Physics and Chemistry of Minerals, 27, 719–731.

Behruzi, M., Hahn, T., Prewitt, C.T., and Baldwin, K. (1984) Low- and high-temperature crystal structures of $LiFeGe_2O_6$, $LiFeSi_2O_6$ and $LiCrSi_2O_6$. Acta Crystallographica A*,* 40 (SUPPL C), 247.

Berman, R.G. (1988) Internally-consistent thermodynamic data for minerals in the system Na_2O-K_2O-CaO-MgO-FeO-Fe_2O_3-Al_2O_3-SiO_2-TiO_2-H_2O-CO_2. Journal of Petrology, 29, 445-522.

Boffa Ballaran T., Nestola F., Tribaudino M., and Ohashi H. (2009) Bulk modulus variation along the diopside–kosmochlor solid solution. European Journal of Mineralogy, 21, 591-597.

Cámara, F., Nestola, F., Angel, R.J., and Ohashi, H. (2009) Spontaneous strain variations through the low-temperature displacive phase transition of $LiGaSi_2O_6$ clinopyroxene European Journal of Mineralogy, 21, 599-614.

Cameron, M., Sueno, S., Prewitt, C.T., and Papike, J.J. (1973) High-temperature crystal chemistry of acmite, diopside, jadeite, spodumene and ureyite. American Mineralogist, 58, 594-618.

Connolly JAD (2005) Computation of phase equilibria by linear programming: A tool for geodynamic modeling and its application to subduction zone decarbonation. Earth and Planetary Science Letters, 236, 524-541.

Davoli, P. (1987) A crystal-chemical study of some aegirin-augites and some evaluations on the oxidation state of Mn. Neues Jahrbuch für Mineralogie - Abhandlungen, 158, 67-87.

Deganello, S. (1973) The thermal expansion of diopside. Zeitschrift für Kristallographie, 137, 127-131.

Dietrich, P., and Arndt, J. (1982) Effects of pressure and temperature on the physical behaviour of mantle-relevant olivine, orthopyroxene and garnet: I. Compressibility, thermal properties and macroscopic Gruneisen parameters. In W. Schreyer, Ed., High-Pressure Researches in Geosciences, p. 293–306. Schweizerbart'sche Verlagsbuchhandlunnngen, Stuttgart.

Downs, R.T., and Hall-Wallace, H. (2003) The American Mineralogist crystal structure database. American Mineralogist, 88, 247-250.

Fei, Y. (1995) Thermal Expansion. In "A handbook of physical constants, mineral physics and crystallography". Ahrens, J.A. (ed). AGU Reference Shelf, 2, 29-44.

Ferrari, S., Nestola, F., Massironi, M., Maturilli, A., Helbert, J, Alvaro, M., Domeneghetti, M.C., and Zorzi F. (2014) In-situ high-temperature emissivity spectra and thermal expansion of C2/c pyroxenes: Implications for the surface of Mercury. American Mineralogist, 99, 786–792.

Finger, L.W., and Ohashi, Y. (1976) The thermal expansion of diopside to 800 °C and a refinement of the crystal structure at 700 °C. American Mineralogist, 61, 303-310.

Frisillo, L.A. and Buljan, S.T. (1972) Linear thermal expansion coefficients of orthopyroxene to 1000 °C. Journal of Geophysical Research, 77, 7115–7117.

Grüneisen, E. (1912) Theorie des festen zustandes einatomizer elemente. Annalen der Physik, 39, 257-306.

Haselton, H.T., Jr., Hemingway, B.S., and Robie, R.A. (1984) Low-temperature heat capacities of $CaAl_2SiO_6$ glass and pyroxene and thermal expansion of $CaAl_2SiO_6$ pyroxene. American Mineralogist, 69, 481-489.

Holland, T.J.B., and Powell, R.T.J.B. (1998) An internally consistent thermodynamic data set for phases of petrological interest. Journal of Metamorphic Geology, 16, 309-343.

Holland, T.J.B. and Powell, R. (2011) An improved and extended internally-consistent thermodynamic dataset for phases of petrological interest, involving a new equation of state for solids. Journal of Metamorphic Geology, 29, 333–388.

Holland, T.J.B., and Redfern, S.A.T. (1997) Unit-cell refinement: Changing the dependent variable and use of regression diagnostics. Mineralogical Magazine, 61, 65-77.

Hovis, G.L., and Graeme-Barber, A. (1997) Volumes of K-Na mixing for low albite – microcline crystalline solutions at elevated temperature. A test of regular solution thermodynamic models. American Mineralogist, 82, 158-164.

Hovis, G.L., Brennan, S., Keohane, M., and Crelling, J. (1999) High-temperature X-ray investigation of sanidine - analbite crystalline solutions: Thermal expansion, phase transitions, and volumes of mixing. The Canadian Mineralogist, 37, 701-709.

Hovis, G.L., Crelling, J., Wattles, D., Dreibelbis, A., Dennison, A., Keohane, M., and Brennan, S. (2003) Thermal expansion of nepheline-kalsilite crystalline solutions. Mineralogical Magazine, 67, 535-546.

Hovis, G.L., Person, E., Spooner, A., and Roux, J. (2006) Thermal expansion of highly silicic nepheline - kalsilite crystalline solutions. Mineralogical Magazine, 70, 383-396.

Hovis, G.L., Morabito, J.R. Spooner, R., Mott, A. Person, E.L., Henderson, C.M.B., Roux, J., and Harlov, D. (2008) A simple predictive model for the thermal expansion of $AlSi_3$ feldspars. American Mineralogist, 93, 1568-1573.

Hovis, G.L., Medford, A., Conlon, M., Tether, A., and Romanoski, A. (2010) Principles of thermal expansion in the feldspar system. American Mineralogist, 95, 1060-1068.

Hovis, G.L., Scott, B.T., Altomare, C.M., Leaman, A.R., Morris, M.D., Tomaino, G.P., and McCubbin, F.M. (2014) Thermal expansion of fluorapatite-hydroxyapatite crystalline solutions. American Mineralogist, 99, 2171-2175.

Hovis, G., Abraham, T., Hudacek, W., Wildermuth, S., Scott, B., Altomare, C., Medford, A., Conlon, M., Morris, M., Leaman, A., Almer, C., Tomaino, G., and Harlov, D. (2015) Thermal expansion of F-Cl apatite crystalline solutions. American Mineralogist, 100, 1040-1046.

Huebner, J.S., and Voigt, D.E. (1988) Electrical conductivity of diopside: Evidence for oxygen vacancies. American Mineralogist, 73, 1235-1254.

Hugh-Jones, D. (1997) Thermal expansion of $MgSiO_3$ and $FeSiO_3$ ortho- and clinopyroxenes. American Mineralogist, 82, 689-696.

Jackson, J.M., Palko, J.W., Andrault, D., Sinogeikin, S.V., Lakshtanov, D.L., Wang, J., Bass, J.D., and Zha, C. (2003) Thermal expansion of natural orthoenstatite to 1473 K. European Journal of Mineralogy, 15, 469-473.

Knight, K.S., and Price, G.D. (2008) Powder neutron-diffraction studies of clinopyroxenes. I: The crystal structure and thermoelastic properties of jadeite between 1.5 and 270 K. Canadian Mineralogist, 46, 1593–1622.

Kòzu S., and Ueda J. (1933) Thermal expansion of diopside. Proceedings of the Imperial Academy, 9, 317-319.

Kroll, H., Kirfel, A., Heinemann, R., and Barbier, B. (2012) Volume thermal expansion and related thermophysical parameters in the Mg, Fe olivine solid-solution series. European Journal of Mineralogy, 24, 935-956.

Kumar, M. (2003) Thermoelastic properties of minerals. Physics and Chemistry of Minerals, 30, 556-558.

Mazzucchelli, M.L., Reali, A., Morganti, S., Angel, R.J., Alvaro, M. (2019) Elastic geobarometry for anisotropic inclusions in cubic hosts. Lithos, 350-351, art. no. 105218,

Murri, M., Alvaro, M., Angel, R.J. , Prencipe M., Mihailova B. (2019) The effects of non-hydrostatic stress on the structure and properties of alpha-quartz. Physics and Chemistry of Minerals, 46, 487–499.

Nénert G., Ingyu Kim, Masahiko Isobe, Clemens Ritter, A. N. Vasiliev, Kee Hoon Kim, Yutaka Ueda (2010) Magnetic and magnetoelectric study of the pyroxene $NaCrSi_2O_6$. Physical Review B, 81, 184408.

Nestola F., Boffa Ballaran, T., Liebske ,C., Bruno, M., and Tribaudino, M. (2006) High-pressure behaviour along the jadeite $NaAlSi_2O_6$ – aegirine $NaFeSi_2O_6$ solid solution up to 10 GPa. Physics and Chemistry of Minerals, 33, 417-425.

Nestola, F., Tribaudino, M., Boffa Ballaran, T., Liebske, C., and Bruno, M. (2007) The crystal structure of pyroxenes along the jadeite - hedenbergite and jadeite - aegirine joins. American Mineralogist, 92, 1492-1501.

Nestola, F., Ballaran, B., Balić-Žunić, T., Secco, L., and Dal Negro, A. (2008). The high-pressure behavior of an Al- and Fe-rich natural orthopyroxene, American Mineralogist, 93, 644-652.

Nestola, F., Boffa Ballaran, T., Angel, R.J., Zhao, J., and Ohashi, H. (2010) High-pressure behavior of Ca/Na clinopyroxenes: The effect of divalent and trivalent 3d-transition elements. American Mineralogist, 95, 832–838

Ohashi, Y. (1982) A program to calculate the strain tensor from two sets of unit-cell parameters. In R.M. Hazen and L.W. Finger, Comparative Crystal Chemistry, p. 92–102. Wiley, Chichester.

Pandolfo, F., Nestola, F., Cámara, F., and Domeneghetti M.C. (2012) New thermoelastic parameters of natural C2/c omphacite. Physics and Chemistry of Minerals, 39, 295-304.

Pandolfo, F., Cámara, F., Domeneghetti, C.M., Alvaro, M., Nestola, F., Karato, S., and Amulele, G. (2015) Volume thermal expansion along the jadeite-diopside join. Physics and Chemistry of Minerals, 42, 1-14.

Parrish, W. (1953) X-ray reflection angle tables for several standards. Technical Report No. **68**, Philips Laboratories Incorporated, Irvington on Hudson, New York.

Pawley, A.R., Redfern, S.A.T., and Holland, T.J.B. (1996) Volume behavior of hydrous minerals at high pressure and temperature: 1. Thermal expansion of lawsonite, zoisite, clinozoisite and diaspore. American Mineralogist, 81, 335–340.

Redhammer, G.J., and Roth, G. (2004) Structural changes upon the temperature dependent C2/*c* → $P2_1/c$ phase transition in $LiMe^{3+}Si_2O_6$ clinopyroxenes, Me = Cr, Ga, Fe, V, Sc and In. Zeitschrift fur Kristallographie, 219, 585-605.

Redhammer, G.J., and Tippelt, G. (2016) The $(Na,Li)FeGe_2O_6$ clinopyroxene-type series: a temperature-dependent single-crystal X-ray diffraction and ^{57}Fe Mössbauer spectroscopic study. Physics and Chemistry of Minerals, 43, 1-22.

Redhammer, G.J., Roth, G., Paulus, W., André, G., Lottermoser, W., Amthauer, G., Treutmann, W., Koppelhuber-Bitschnau, B. (2001) The crystal and magnetic structure of Li-aegirine $LiFe^{3+}Si_2O_6$: A temperature-dependent study. Physics and Chemistry of Minerals, 28, 337-346.

Redhammer, G., Amthauer, G., Roth, G., Tippelt, G., and Lottermoser, W. (2006) Single-crystal X-ray diffraction and temperature dependent ^{57}Fe Mössbauer spectroscopy on the hedenbergite-aegirine $(Ca,Na)(Fe^{2+},Fe^{3+})Si_2O_6$ solid solution. American Mineralogist, 91, 1271-1292.

Redhammer, G.J., Cámara, F., Alvaro, M., Nestola, F., Tippelt, G., Prinz, S., Simons, J., Roth, G., Amthauer, G. (2010) Thermal expansion and high-temperature $P2_1/c$-$C2/c$ phase transition in clinopyroxene-type $LiFeGe_2O_6$ and comparison to $NaFe(Si,Ge)_2O_6$. Physics and Chemistry of Minerals, 37, 685-704.

Redhammer, G.J., Senyshyn, A., Tippelt, G., Prinz, S., and Roth, G. (2015) Structural and magnetic phase transitions in the synthetic clinopyroxene $LiCrGe_2O_6$: a neutron diffraction study between 0.5 and 1473 K. Physics and Chemistry of Minerals, 42, 491-507.

Redhammer, G.J., Senyshyn, A., Lebernegg, S., Tippelt, G., Dachs, E., and Roth, G. (2017) A neutron diffraction study of crystal and low-temperature magnetic structures within the $(Na,Li)FeGe_2O_6$ pyroxene-type solid solution series. Physics and Chemistry of Minerals, 44, 669-684.

Richet, P., Mysen, B. and Ingrin, J. (1998) High-temperature X-ray diffraction and Raman spectroscopy of diopside and pseudowollastonite. Physics and Chemistry of Minerals, 25, 401–414.

Salje, E. K. H., Wruck, B., and Thomas, H. (1991) Order-parameter saturation and low-temperature extension of Landau theory. Zeitschrift für Physik B–Condensed Matter, 82, 399-404.

Sarver, J.F., and Hummel, F.A. (1962) Stability relations of magnesiummetasilicate polymorphs. Journal of the American Ceramic Society, 45, 152–157.

Scandolo, L., Mazzucchelli, M., Alvaro, M., Nestola, F., Pandolfo, F., and Domeneghetti, M. (2015)

Thermal expansion 36behavior of orthopyroxenes: The role of the Fe-Mn substitution. Mineralogical Magazine, 79, 71-87.

Schaller, W. (1938) Johannsenite, a new manganese pyroxene. American Mineralogist, 23, 575-582.

Smyth J.R. (1973) An orthopyroxene structure up to 850°C. American Mineralogist, 58, 636–648.

Solomatova, N.V., Alieva, A., Finkelstein, G.J, Sturhahn, W., Baker, M.B., Beavers, C.M., Zhao, J., Toellner, T.S., and Jackson J.M. (2019) High-pressure single-crystal X-ray diffraction and synchrotron Mössbauer study of monoclinic ferrosilite, Comptes Rendus Geoscience, 351, 129-140.

Sueno, S., Cameron, M., and Prewitt, C.T. (1976) Orthoferrosilite: high temperature crystal chemistry. American Mineralogist, 61, 38-53.

Suzuki, I., Okajima, S., and Seya, K. (1979) Thermal expansion of single-crystal manganosite. Journal of Physics of the Earth, 27, 63–69.

Tennant, W.C., McCammon, C.A., and Miletich, R. (2000) Electric-field gradient and mean-squared-displacement tensors in hedenbergite from single-crystal Mössbauer milliprobe measurements. Physics and Chemistry of Minerals, 27, 156-162.

Thompson, R.M., and Downs, R.T. (2004) Model pyroxenes II: Structural variation as a function of tetrahedral rotation. American Mineralogist, 89, 614-628.

Thompson, R.M., and Downs, R.T. (2008). The crystal structure of diopside at pressure to 10 Gpa. American Mineralogist, 93, 177-186.

Tribaudino M. (1996) High-temperature crystal chemistry of *C*2/*c* clinopyroxenes along the join $CaMgSi_2O_6$-$CaAl_2SiO_6$. European Journal of Mineralogy, 8, 273-279.

Tribaudino, M., and Mantovani, L. (2014) Thermal expansion in *C*2/*c* pyroxenes: a review and new high temperature structural data on a pyroxene of composition $(Na_{0.53}Ca_{0.47})(Al_{0.53}Fe_{0.47})Si_2O_6$ ($Jd_{53}Hd_{47}$). Mineralogical Magazine, 78, 311-324.

Tribaudino M., Prencipe, M., Bruno, M., and Levy D. (2000) High pressure behaviour of Ca-rich *C*2/*c* clinopyroxenes along the join diopside-enstatite ($CaMgSi_2O_6$-$MgSi_2O_6$). Physics and Chemistry of Minerals, 27, 656-664.

Tribaudino, M., Nestola, F., Cámara, F., and Domeneghetti, M.C. (2002) The high temperature $P2_1/c$-*C*2/*c* phase transition in Fe-free pyroxene ($Ca_{0.15}Mg_{1.85}Si_2O_6$): structural and thermodynamic behavior. American Mineralogist, 87, 648-657.

Tribaudino, M., Nestola, F., Prencipe, M., and Rundlof, H. (2003) A single-crystal neutron-diffraction investigation of spodumene at 54 K. Canadian Mineralogist, 41, 521-527.

Tribaudino, M., Bruno, M., Iezzi, G., Della Ventura, G., and Margiolaki, I. (2008a) The thermal behavior of richterite. American Mineralogist, 93, 1659–1665.

Tribaudino, M., Nestola, F., Bruno, M., Boffa Ballaran, T., and Liebske, C. (2008b) Thermal expansion along the $NaAlSi_2O_6$-$NaFe^{3+}Si_2O_6$ and $NaAlSi_2O_6$-$CaFe^{2+}Si_2O_6$ solid solutions. Physics and Chemistry of Minerals, 35, 241-248.

Tribaudino, M., Bromiley, G., Nestola, F., and Ohashi, H. (2009) Synthesis, TEM characterization and high temperature behaviour of $LiNiSi_2O_6$ pyroxene. Physics and Chemistry of Minerals, 36, 527-536.

Tribaudino, M., Bruno, M., Nestola, F., Pasqual, D., and Angel, R.J. (2011) Thermoelastic and thermodynamic properties of plagioclase feldspars from thermal expansion measurements. American Mineralogist, 96, 992-1002.

Wallace, D.C. (1998) Thermodynamics of Crystals, 512 p., Dover Publications, New York.

Xu, Z., Ma, M., Li, B., and Hong, X., (2019) Compressibility and thermal expansion of natural clinopyroxene $Di_{0.66}Hd_{0.13}Jd_{0.12}Ts_{0.05}$. Results in Physics, 12, 447-453.

Yang, H., and Ghose, S. (1994) Thermal Expansion, Debye temperature and Grüneisen parameter of synthetic (Fe, Mg)SiO_3 orthopyroxenes. Physics and Chemistry of Minerals, 20, 575-586.

Zaffiro, G., Angel, R.J., Alvaro, M. (2019) Constraints on the Equations of State of stiff anisotropic minerals: Rutile, and the implications for rutile elastic barometry Mineralogical Magazine, 83, 339-347.

Zhang, Li, Ahsbahs, H., Hafner, S.S., and Kutoglu, A. (1997) Single-crystal compression and crystal structure of clinopyroxene up to 10 Gpa. American Mineralogist, 82, 245–258.

Zhao, Y., Schiferl, D., and Shankland, T.J. (1995) A high P-T single-crystal X-ray diffraction study of thermoelasticity of $MgSiO_3$ orthoenstatite. Physics and Chemistry of Minerals, 22, 393–398.

Zhao, Y., Von Dreele, R.B., Shankland, T.J., Weidner, D.J., Zhang, J., Wang, Y., and Gasparik, T. (1997) Thermoelastic equation of state of jadeite $NaAlSi_2O_6$: an energy-dispersive Rietveld refinement study of low symmetry and multiple phases diffraction. Geophysical Research Letters, 24, 5-8.

FIGURE CAPTIONS

Figure 1: (a) volume and (b) thermal expansion coefficient vs. temperature for jadeite based on different models. Fits utilized data at $T \geq 298$ K from present work only.

Figure 2: Unit-cell volume data used in the Kroll fits, except for johannsenite high-T data represented by less-prominent diamonds. Volume data at $T \geq 298$ K are from the current work. Sources and symbols for the low-temperature data are: hedenbergite full blue diamonds (Redhammer et al. 2010), aegirine open blue diamonds (Redhammer et al. 2010), kosmochlor open red diamond (Nenert et al. 2010), spodumene open magenta diamond (Tribaudino et al. 2003).

Figure 3: (a) Thermal expansion coefficient at $T = 1073$ K according to the empirical Fei vs. the physical Kroll model. Red circles are for orthopyroxenes, diamonds for clinopyroxenes, green Na-pyroxenes, dark green omphacite, purple spodumene, and black Ca-pyroxenes. The line indicates the

ideal plot if coefficients were the same for the two models. (b) Volume thermal expansion for enstatite comparing the Fei and Kroll models based on fits to the same data.

Figure 4: V/V_0 vs. T for orthoenstatite and orthoferrosilite from data of previous investigations and also current work.

Figure 5: Volume and volume thermal expansion in orthopyroxenes vs. absolute temperature based on present work and the data of Yang and Ghose (1994), as discussed in the text.

Figure 6: Linear thermal expansion coefficient of orthoenstatite along the series orthoenstatite-orthoferrosilite.

Figure 7: V/V_0 vs. T for (a) diopside and (b) hedenbergite. (c) Thermal expansion coefficients for diopside, hedenbergite, and johannsenite.

Figure 8: Unit-cell parameter a vs. T for johannsenite of the present study. Note that the linear trend becomes irregular above ~400 °C.

Figure 9: (a) V/V_0 vs. T for jadeite based on data from both present and previous investigations and (b) volume thermal expansion coefficient for jadeite and omphacite compared with diopside (K' = 6.8); all data from present work.

Figure 10: (a) V/V_0 vs. T for aegirine based on data from present and previous investigations and (b) comparison of volume thermal expansion coefficients for jadeite, aegirine, and kosmochlor.

Figure 11: Variation of volume thermal expansion coefficient with temperature for spodumene vs. jadeite.

Figure 12: Linear thermal expansion coefficient in synthetic pyroxenes along the series diopside - Ca-Tschermak pyroxene. Data are from Haselton et al. (1984) for Ca-Tschermak, Tribaudino (1996) for intermediate compositions, and present work for diopside.

Figure 13: Thermal expansion coefficient at 298 K vs. unit-cell volume (halved for orthopyroxenes) based on present data.

Figure 14: Changes in the components of thermal strain with temperature in clinopyroxenes.

Figure 15: Higher deformation (second highest) on (010) at low and high temperature, calculated (a) between T = 298 and 748 K and (b) between T = 748 and 1073 K. The length of the sticks is proportional to the deformation on (010). Only the higher deformation axis is shown, as the other is normal to the page. High-temperature data for hedenbergite and johannsenite are not shown, as data in the high-temperature range are either missing or affected by phase transformation (see text).

Figure 16: Unit-cell parameters with temperature for (a) enstatite and (b) $En_{75}Fs_{25}$. The arrow indicates turnover in the b and c parameters for $En_{75}Fs_{25}$, possibly related to a phase transition.

Figure 17: Thermal tensor coefficients for present enstatite and $En_{75}Fs_{25}$ samples, as well as the $Di_{15}En_{85}$ synthetic pyroxene of Tribaudino et al. (2002), as discussed in the text.

This is the peer-reviewed, final accepted version for American Mineralogist, published by the Mineralogical Society of America.
The published version is subject to change. Cite as Authors (Year) Title. American Mineralogist, in press.
DOI: https://doi.org/10.2138/am-2021-7650. http://www.minsocam.org/

REVISED FIGURE 7

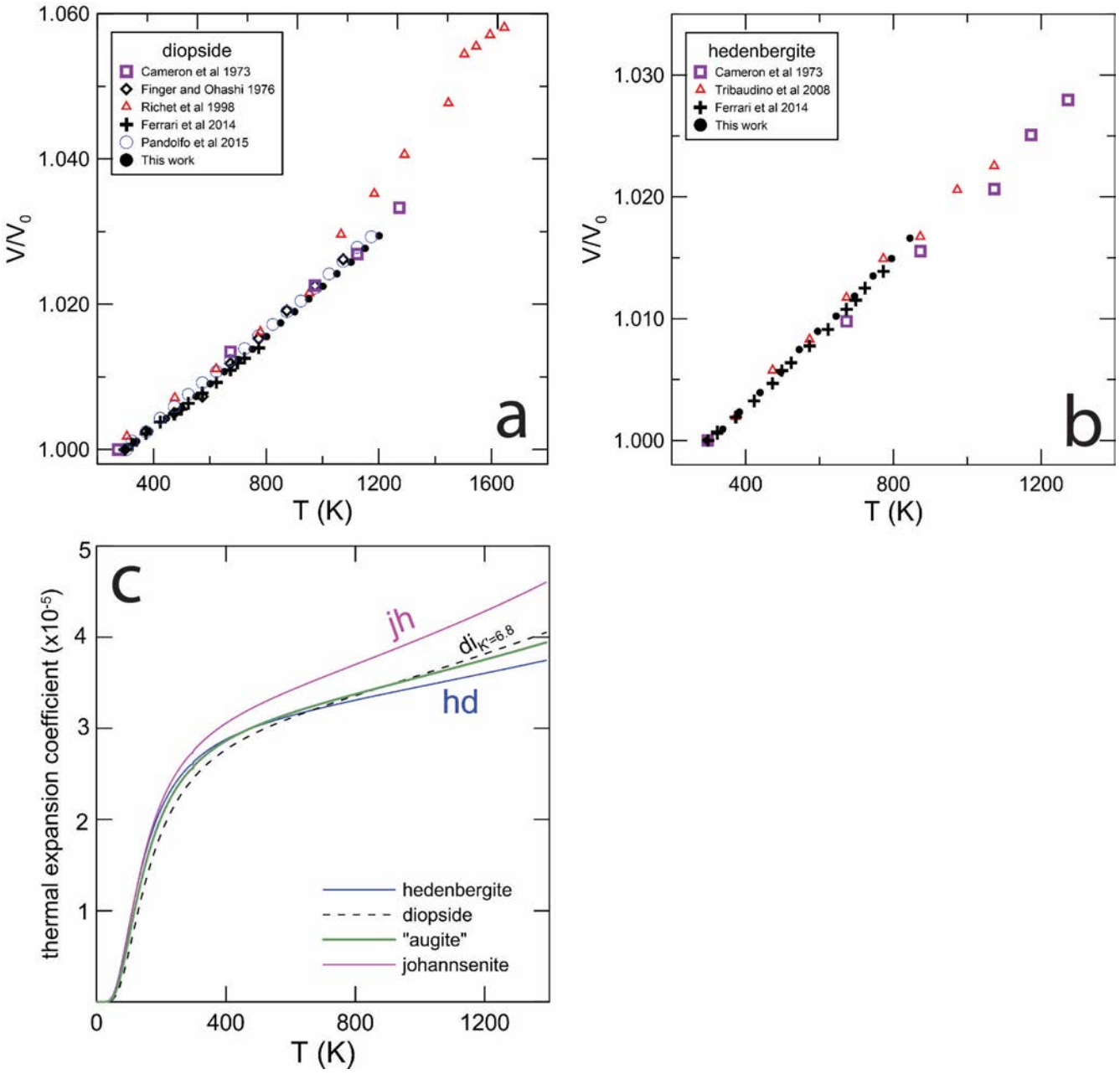

This is the peer-reviewed, final accepted version for American Mineralogist, published by the Mineralogical Society of America.
The published version is subject to change. Cite as Authors (Year) Title. American Mineralogist, in press.
DOI: https://doi.org/10.2138/am-2021-7650. http://www.minsocam.org/

REVISED FIGURE 8